Electronic Supplementary Material (ESI) for Nanoscale.

Supplementary Information to

The effect of biomolecular corona on adsorption onto and desorption from a model lipid membrane

Ceri J. Richards,[a,b] Majid Ahmadi,[c] Marc C. A. Stuart,[d] Bart J. Kooi,[c] Christoffer Åberg,[*b] Wouter H. Roos [*a]

[a] Molecular Biophysics, Zernike Institute for Advanced Materials, Rijksuniversiteit Groningen, 9747 AG Groningen, Netherlands

[b] Pharmaceutical Analysis, Groningen Research Institute of Pharmacy, Rijksuniversiteit Groningen, 9713 AV Groningen, Netherlands

[c] Nanostructure Materials and Interfaces, Zernike Institute for Advanced Materials, Rijksuniversiteit 9747 AG Groningen, Groningen, Netherlands

[d] Department of Electron Microscopy, Groningen Biomolecular Sciences and Biotechnology Institute, Rijksuniversiteit Groningen, 9747 AG Groningen, Netherlands

[*]Email: w.h.roos@rug.nl

[*]Email: christoffer.aberg@rug.nl

Particle characterization

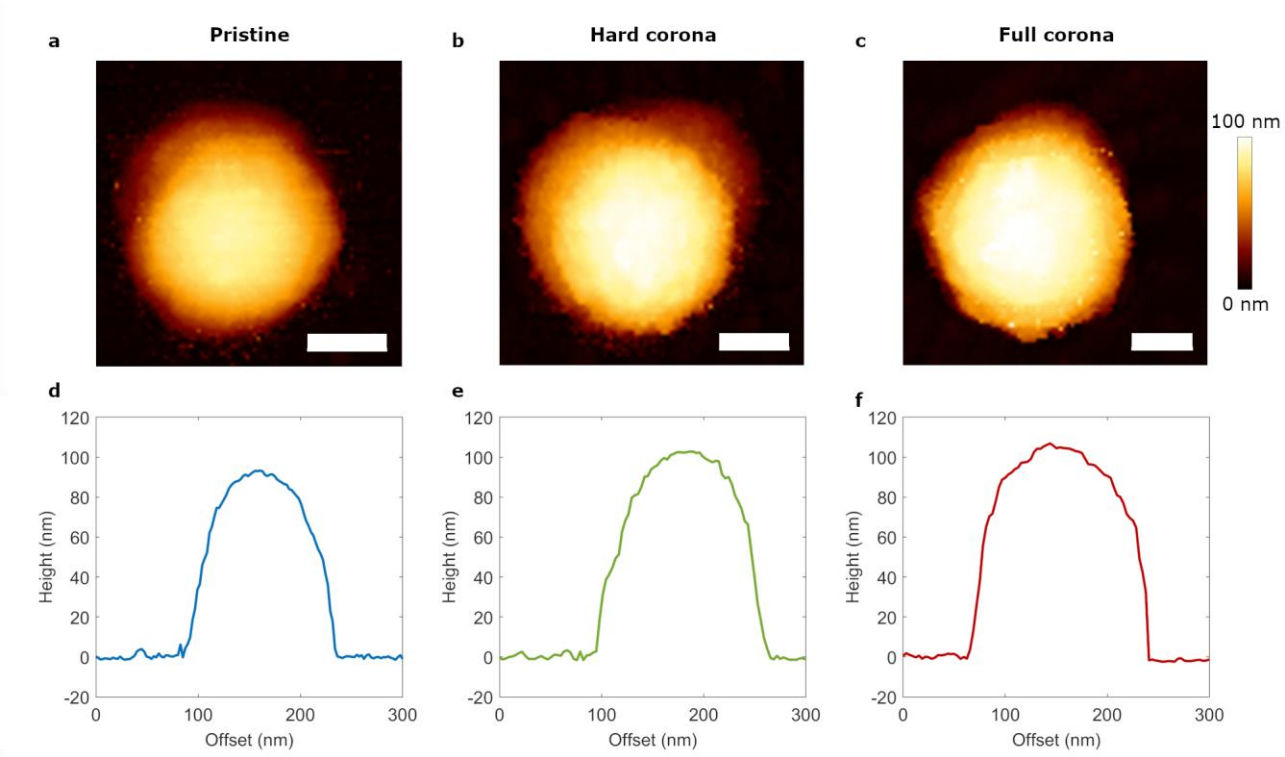

Supplementary Figure S1. Characterization of 100 nm carboxylated polystyrene particles under various corona conditions by atomic force microscopy. Atomic force microscopy images of a **a,** pristine; **b,** hard corona-covered; and **c,** full corona particle. Colour indicates height above the substrate. Scale bars represent 50 nm. Corresponding height profiles at the centre of the particles are given in **d-f.** The height profiles were used to yield particle height data.

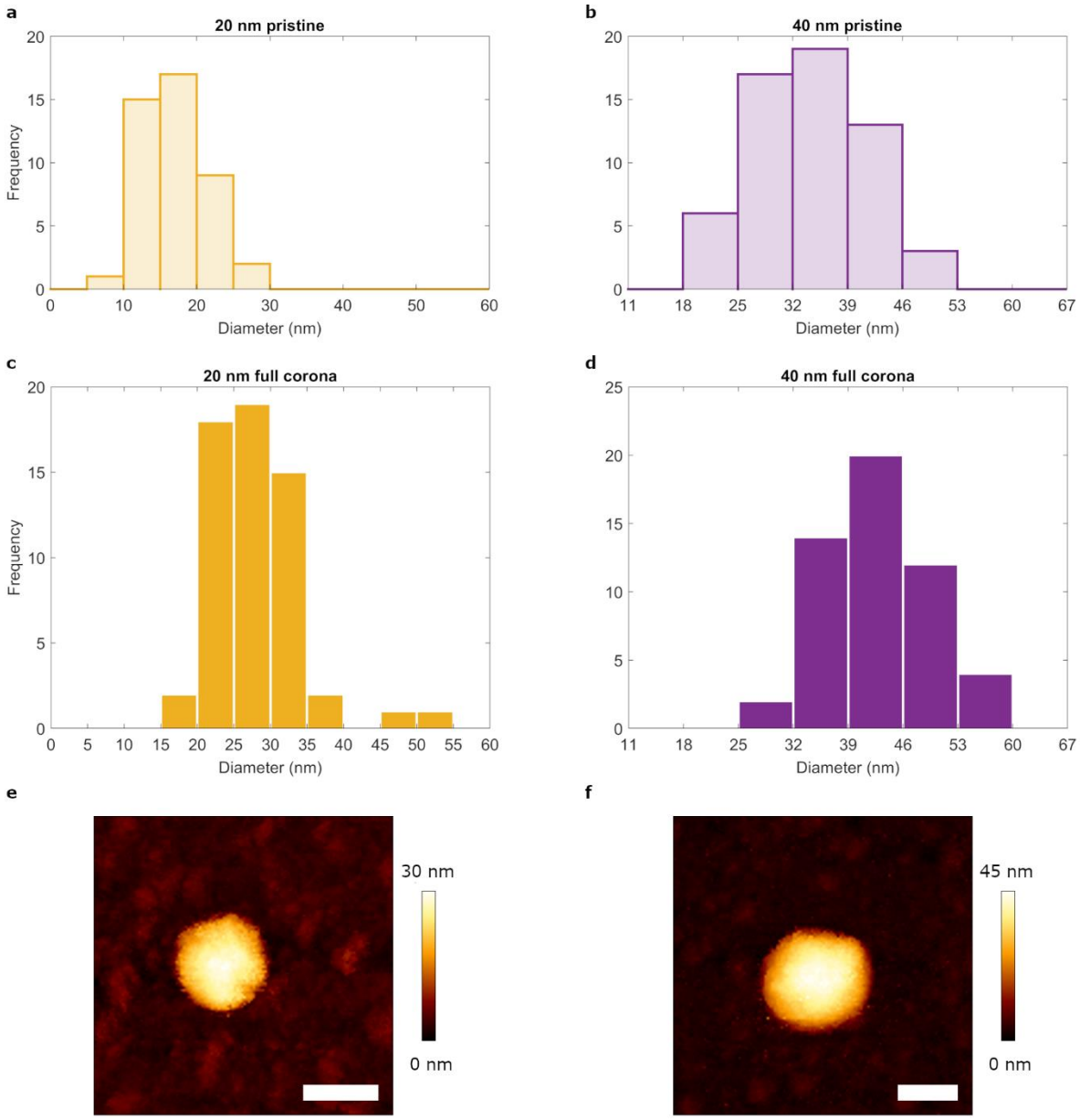

Supplementary Figure S*2*. Size characterization of 20 nm and 40 nm carboxylated polystyrene particles. Particle size distributions from atomic force microscopy imaging of **a,** 20 nm pristine; **b,** 40 nm pristine; **c,** 20 nm full corona; and **d,** 40 nm full corona particles. Particle height data was obtained from line profiles of the atomic force microscopy images and used for the particle diameters. This yielded average particle diameters of 17.1 ± 0.7 nm and 34.0 ± 0.9 nm for 20 nm and 40 nm pristine particles, respectively, and 27.9 ± 0.8 nm and 43 ± 1 nm for 20 nm and 40 nm full corona particles, respectively. Representative atomic force microscopy images of **e,** 20 nm full corona; and **f,** 40 nm full corona particles. Colour indicates height above the substrate. Scale bars represent 50 nm.

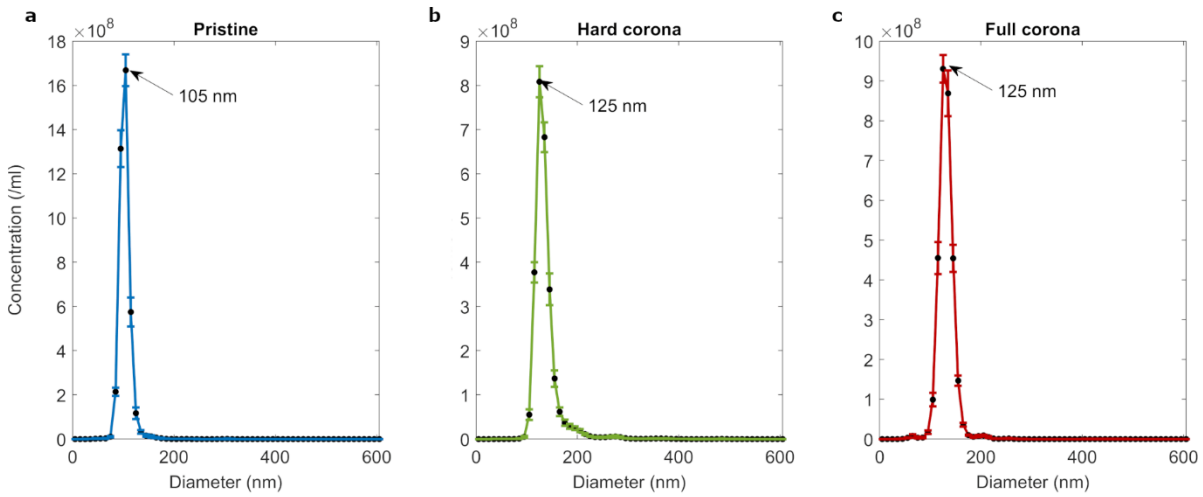

Supplementary Figure S3. Size characterization of 100 nm carboxylated polystyrene particles under various corona conditions by nanoparticle tracking analysis. Particle size distributions from nanoparticle tracking analysis of **a,** pristine; **b,** hard corona-covered; and **c,** full corona particles. Particle trajectories were collected and analysed using the NTA 3.0 software, which determines the hydrodynamic diameter based on the diffusion coefficient associated with the particle trajectory. The number of particles of a given diameter was normalized by the sample volume to calculate the concentration of particles of that size within the sample. The error bars show the standard error for 5 technical replicates. All particle preparations showed narrow peaks indicating limited polydispersity. Pristine particles had a peak maximum at 105 nm whereas both corona preparations had *peak* hydrodynamic diameters of 125 nm. The mean diameters were 98 ± 12 nm, 131 ± 27 nm and 126 ± 16 nm for pristine, hard corona-covered and full corona particles, respectively.

Imaging the biomolecular corona with liquid cell STEM

The experimental set up for the liquid cell scanning transmission microscopy experiments is presented in Supplementary Fig. S4a. Quantifoil grids were backed with graphene grown on Cu foil. Attachment to the graphene was improved using isopropyl alcohol (IPA). The Cu foil was subsequently etched away and the grids were washed. Particle dispersion was placed on the lower grid and left to partially dry to remove excess liquid. Another Quantifoil grid backed with graphene was then placed on top and the grids were sandwiched together. In the regions where the grid holes overlapped (as indicated by the white arrow, centre of Supplementary Fig. S4b) "cells" between only the two graphene sheets were formed. The cells were isolated from the vacuum and contained small volumes of water where particles were trapped between the graphene layers, as schematically represented in the top right of Supplementary Fig. S4a. The bottom right shows a graphical representation of the expected scanning electron microscopy image of a particle within the liquid cell. A bright gradient beginning partially within the particle region and reducing in contrast with distance from the particle is expected due to the small volume of water trapped around the particle and between the graphene sheets. Small volumes within the undercut of the particle and graphene sheet were expected to produce a contrast that increased to a maximum just beyond the particle edge where the water volume would be thickest, followed by a decrease in contrast as the water layer reduced. Supplementary Fig. S4b shows a pristine nanoparticle imaged with this method. This image looks very similar to the expected image for a particle trapped in a liquid containing cell. Supplementary Fig. S4c shows a zoomed in section of the particle where, other than the anticipated contrast gradient, no structure could be observed on the particle. Supplementary Fig. S4d shows a hard corona-covered particle. A contrast gradient due to entrapped water was also present but, in addition, material can also be seen on the particle surface (white arrow, Supplementary Fig. S4e). As preparations were similar to the cryogenic electron microscopy experiments, we suggest that this material is the biomolecular coating.

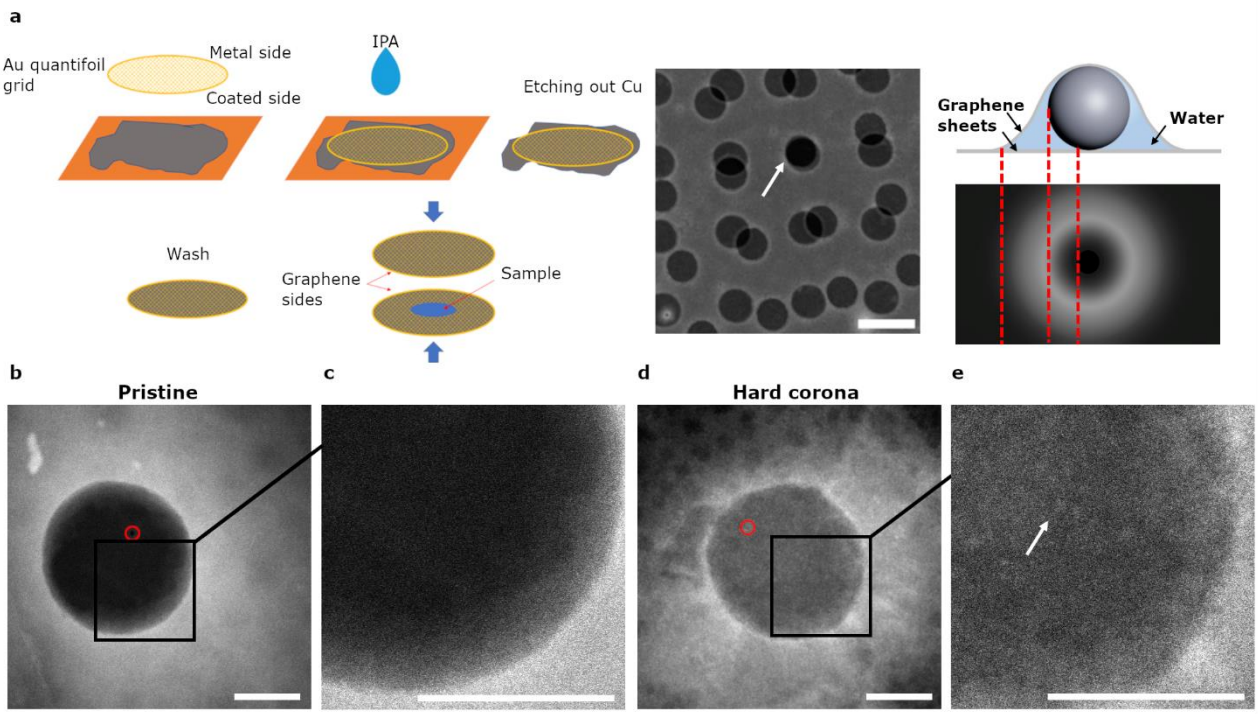

Supplementary Figure S4. Characterization of 100 nm carboxylated polystyrene particles under various corona conditions by liquid scanning transmission microscopy. a, Experimental set up for the liquid scanning transmission microscopy experiments. Left shows the procedure for backing the grids with graphene sheets. Graphene was deposited using chemical vapor deposition onto Cu foil. The grids were then placed coated side down onto the graphene sheets and IPA was used to ensure attachment. The Cu foil was etched away and the grids were washed. Particle dispersion was placed on one grid and another grid was sandwiched on top to produce particle solution containing cells. Centre shows a scanning transmission electron microscopy image of the grid stack in which regions where the holes in the Quantifoil grids overlapped, indicated by the white arrow, were investigated to find particles trapped between the graphene (scale bar represents 2 μm). Schematic illustration of the entrapped water surrounding the particles (top right) and the expected intensity profile produced by such a configuration (bottom right) . **b,** Pristine nanoparticles showed a bright gradient attributed to the small volume of water trapped around the particle. **c,** zoom in of the particle in b, no structure on the particle surface can be seen. **c,** Image of a hard corona-covered particle and zoom-in in **d**. A contrast gradient due to entrapped water was also present but, in addition, material can also be seen on the particle surface. Red circles indicate where the beam spot was placed, therefore features here are most likely caused by beam damage. Scale bars represent 50 nm.

Statistical Evaluation of residence times

Supplementary Table S1. Proportion of long lived events under various particle conditions. The first row of the table lists the proportion of events that resided for 120 s or more, obtained from pooling the data from all repeat measurements of the same particle condition. The second row lists the averaged value of the proportion of events with 120s or more duration for the separate trials of the same particle condition. The standard deviation was calculated using equal weights for each repeat.

	100 nm pristine	100 nm hard corona	100 nm hard corona with preincubation	100 nm full corona	40 nm full corona	20 nm full corona
Proportion of events that were resident for 120 s or more (pooled data)	0.71	0.06	0.2	0.002	0.02	0.03
Average proportion of events that were resident for 120 s or more for the separate trials ± standard deviation	0.71 ± 0.18	0.06 ± 0.02	0.25 ± 0.18	0.003 ± 0.004	0.06 ± 0.08	0.03 ± 0.03

Supplementary Table S2. Statistical comparison of the residence time distributions. Two sample Kolmogorov-Smirnov tests were performed using the pooled residence time distributions of the various particle conditions. Data sets were compared using the null hypothesis that the two samples came from the same distribution. *p*-values of <0.05 indicate data sets for which the null hypothesis was rejected at a 5% confidence interval. 100 nm particles under various corona conditions where compared to each other, and full corona particles of different sizes were compared. Empty cells represent identical conditions (*e.g.*, 100 nm hard corona compared to itself) or less relevant comparisons (*e.g.*, 100 nm hard corona to 40 nm full corona).

Sample 1 / Sample 2	100 nm pristine	100 nm hard corona	100 nm full corona	40 nm full corona	20 nm full corona
100 nm hard corona	$p < 0.05$		$p < 0.05$		
100 nm full corona	$p < 0.05$	$p < 0.05$		$p < 0.05$	$p = 0.92$
40 nm full corona			$p < 0.05$		$p = 0.27$

Particle adsorption rates onto lipid bilayers

Calculation of rates

The adsorption rates were calculated for each particle condition from the number of adsorption events across the experiment timespan, shown in Supplementary Figure S5. For all particles under corona conditions, the adsorption rate was approximately uniform across the experiment timespan. Therefore, the adsorption rate was calculated using the number of events observed divided by the experiment duration (10 mins) and the area of the field of view. For 100 nm pristine particles, we observed a time dependent adsorption rate, with more events occurring at early times within the experiment. This time dependence could be as a result of, for example, depletion of the number of particle in the bulk solution or increased occupancy of the bilayer resulting in fewer binding sites. Therefore, we chose to calculate an upper estimate of the pristine particle adsorption rate using the first 60 s of the experimental data, where these effects would still be minimal. The results are shown in Table 1.

Kinetic theory suggests that the expected collision rate of nanoparticles with the membrane is given by:

$$\sqrt{\frac{k_B T}{2\pi m_p}}\, n$$

where k_B is the Boltzmann constant, T is the absolute temperature, m_p the particle mass and n the number density of particles at the membrane. The same result may be found by solving the Klein-Kramers equation[1] for a uniform system at equilibrium with a reflecting surface. Assuming the absence of interactions, we can estimate the local number density of particles with the average number density (0.5×10^9 ml^{-1}). Particle masses were calculated using the nominal diameters and density of polystyrene (1.05 g/ml) yielding 4.4×10^{-21} kg, 3.5×10^{-20} kg, and 5.5×10^{-19} kg for 20 nm, 40 nm and 100 nm particles, respectively. The results are shown in Table 1.

The propensity to sediment was estimated using Stokes' law to determine the terminal velocity of the particles in water.[2] Multiplying this by the total experiment time yielded the distance covered in the z direction by a falling particle. Using the number density of particles, n, and the area of the field of view, the total number of particles that would sediment into the observation region during the experiment due to gravitational effects was calculated. The results are shown in Supplementary Table S3.

Supplementary Table S3. Estimated sedimentation rates. See above for calculation. The table lists the number of particles expected to sediment onto the lipid bilayer within the observation region and time (10 mins) of the experiments for a given particle size. This should be compared to the number of adsorption events observed per trial. In all cases this was much greater than the expected sedimentation rate, highlighting that the effect of sedimentation was negligible.

	100 nm	40 nm	20 nm
Expected number of particles to sediment	1.8	0.2	0.0

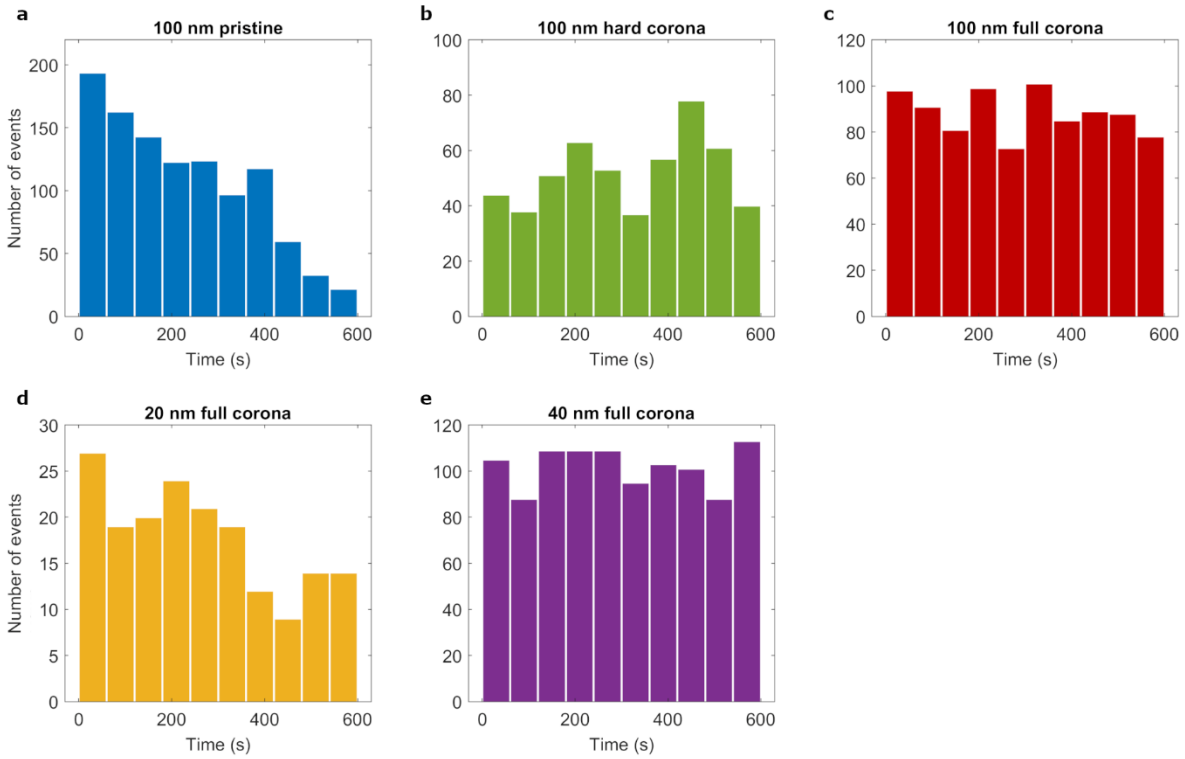

Supplementary Figure S5. Adsorption rates of carboxylated polystyrene particles on lipid bilayers. **a–c,** 100 nm particles; **a,** pristine; **b,** hard corona-covered; and **c,** full corona. **d,** 20 nm full corona particles. **e,** 40 nm full corona particles. The histogram represents the number of particles that adsorbed within a given minute within the observation period of the experiment. The data set was obtained by pooling the adsorption times from repeat measurements of the same conditions. Therefore, due to the different number of repeats performed per condition (minimally 5 in all cases), the magnitude of the total number of events must be converted into the average number per trial, as well as corrected for the usage of different concentrations for the different particle sizes in order to quantitatively compare adsorption rates. See Table 1 of the main text for numbers where this correction has indeed been performed. The above graphs instead offer information on the trend of the adsorption rate *across time*. All corona particle conditions exhibit nominally a uniform number of adsorption events across time, noting that the 20 nm full corona particles yielded fewer events and therefore small number fluctuations were expected to be relatively more influential. 100 nm pristine particles showed a decrease in number of adsorption events across time.

Bilayer incubation with complete medium

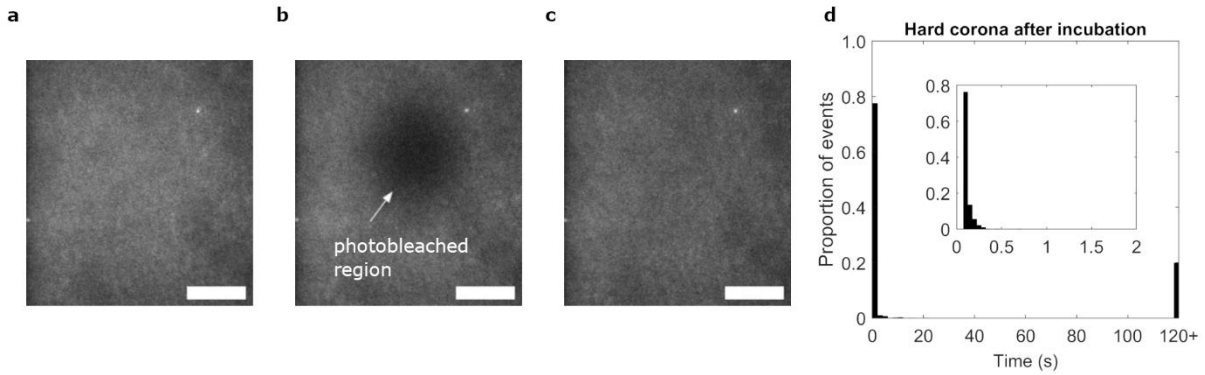

Supplementary Figure S6. Effects of biomolecule adsorption onto lipid bilayers. Bilayers were incubated with complete cell culture medium for 1 h followed by quickly washing with phosphate buffer saline. Photobleaching was then performed to assess whether bilayer fluidity was maintained after this procedure. Images of fluorescently labelled lipid bilayers **a,** before photobleaching; **b,** immediately after photobleaching; and **c,** 5 min after photobleaching. All scale bars represent 20 µm. Full recovery of the fluorescence signal within the photobleached region was achieved, indicating that the bilayer continued to be fluid after biomolecule incubation. **d,** Residence time distribution of hard corona-covered particles added to lipid bilayers that had undergone the incubation procedure. Particles adsorbed onto lipid bilayers for 120 s or more are represented by the final bar of the plot (120+). The proportion of the data within the 120+ bin is increased compared to the condition of hard corona-covered particles on bilayers without the incubation procedure. The inset shows the sub 2 s residence time distributions with smaller (50 ms) bins. However, the preincubation also led to a decrease in the reproducibility of the results, evidenced by the increase in the standard deviation across the repeats (Supplementary Table 1). It is worthwhile noting that this experiment did not assess the effect of biomolecules weakly bound to the bilayer as they would have been removed by the washing procedure.

Threshold values for residence time distributions

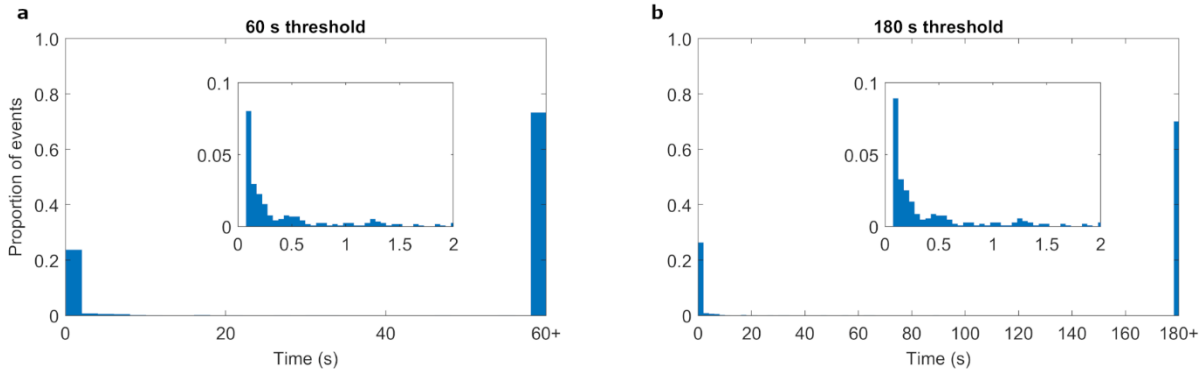

Supplementary Figure S7. Residence times with various thresholds of the 100 nm pristine particles at the lipid bilayer. Particles adsorbed on the bilayer were defined as stationary bright spots visualized by fluorescence microscopy. A residence time was associated with each adsorption event, i.e., the duration that the stationary spot was present on the bilayer. Histograms of the pooled residence time distributions from repeat trials of pristine particles using threshold values of **a,** 60 s; and **b,** 180 s. Particles adsorbed to the lipid bilayer for the threshold value or more are represented by the final bars. The distributions do not differ greatly from each other nor do they differ from those resulting from the 120 s threshold presented in the main text (Fig. 3a).

Analysis of microscopy videos

Background subtraction

Due to the higher laser power required to image the 20 nm particles, a significant background was observed because of cross-talk between the nanoparticle and lipid bilayer channel. Thus, background subtraction was performed in order to distinguish the particles more readily. A Gaussian blur filter with a 15 pixel radius (corresponding to 4.69 µm) was applied to each image of the video. This was then subtracted from the original data, after which analysis was performed on the result. Background subtraction was not performed on the 40 nm and 100 nm particle data.

Particle tracking

In order to obtain the residence time of single particles on lipid bilayers, the particle tracking plugin TrackMate from ImageJ/Fiji was used.[3–5] Particle identification was performed with the Difference of Gaussians (DoG) detector, using a blob diameter of 4 pixels (corresponding to 1.25 µm) for the 100 nm particles and 3 pixels (corresponding to 0.94 µm) for the 20 nm and 40 nm particles. Median filtering and sub pixel localization was applied. The detection threshold was set so that particles were appropriately identified after visual inspection. After identifying particles in all images in this way, identified particles were linked across time using the Simple LAP Tracker. It was necessary to differentiate between particles that were adsorbed onto the bilayer compared to those diffusing in the solution within 200 nm of the bilayer surface, as both cases may be visualized using total internal fluorescence microscopy. Therefore, we chose to only consider particles as adsorbed to the bilayer if they did not appreciably move between frames, in other words, particles that appeared to be stationary. We defined stationary events by using a maximum linking distance of 1 pixel (corresponding to 312.5 nm) for the Simple LAP Tracker. It is worthwhile noting that particles could potentially adsorb and move around in the plane of the bilayer. These events are not included in our analysis of particle-bilayer interactions.

After automated particle linking, manual correction was performed for particles that were misidentified, i.e., particles on the bound of the threshold resulting in several separate events as opposed to one (or none if the particle signal was in general low). Intensity profiles were calculated by averaging the intensities of a 5x5 pixel square centred on the particle position, plotted against time. The intensity profiles where then visually inspected to check for any further anomalous behaviour leading to possible misidentification. For instance, in the case of a moving particle some stationary segments may be identified. The intensity profile of those segments would show a broader peak than the residence time ascribed from the particle tracking, due to the particle moving in the vicinity contributing fluorescence signal to the surrounding region. Supplementary Fig. 8 shows an example of the broadened peak of a moving particle. Candidates for misidentification were then visually inspected in the original raw data. Any moving particles were removed from the data set.

Notably, some of the intensity profiles showed step-like traces as in Supplementary Fig. 8. It was found that in many cases this was due to the particle moving or the adsorption/desorption of neighbouring particles, altering the local background intensity. However, the steps in some profiles could not be ascribed to these factors. The intensity steps could be attributed to small movements in the plane perpendicular to the sample if, for example, a pore in the bilayer formed beneath the particle adsorption site, thereby bringing the particle closer to the glass. The ratio of the measured intensities (I_1 / I_2) of an object at height 1 and 2 (z_1 and z_2 respectively) from the interface under

conditions of total internal reflection is given by the following equation

$$\frac{I_1}{I_2} = e^{\frac{z_1 - z_2}{d}}$$

where *d* is the penetration depth of the beam. However, the ratio was much greater for the measured data than that theoretically expected for a height change corresponding to the bilayer thickness, ~ 5 nm. With no reasonable explanation for the large observed steps, no further analysis of the intensities was conducted. Finally, events of minimally 3 frames were used and ascribed a residence time given by the difference between the adsorption time point and the desorption time point.

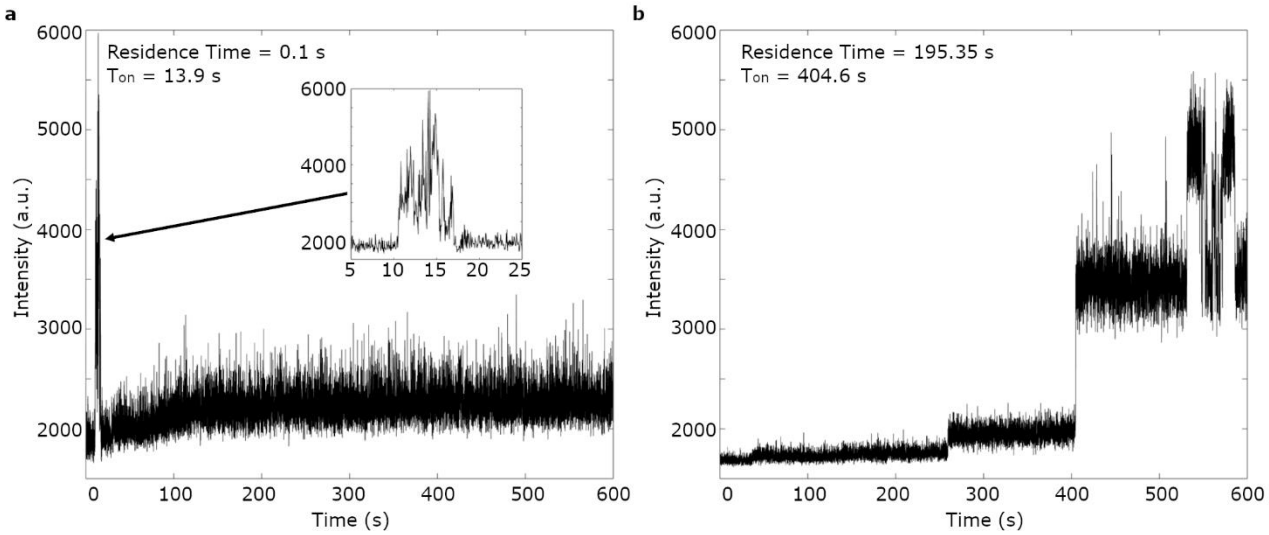

Supplementary Figure S8. Example intensity profiles of stationary particles. Intensity profiles of 100 nm pristine particles **a,** for a particle which was ascribed a stationary residence time of 0.1 s by the initial analysis. The inset shows the intensity profile in the vicinity of the adsorption time (T_{on}) at 13.9 s after the beginning of the measurement. No clear, isolated signal peak of 0.1 s is apparent. On further inspection of the raw data the particle was found to traverse the bilayer. **b,** Intensity profile of a particle that shows step-like features after the initial adsorption event at 404.6 s. Review of the raw data showed that the particle remained stationary within the plane of the bilayer from the initial adsorption event until the end of the measurement period.

Supplementary microscopy videos

Supplementary video 1: SupplementaryVideo_S1_Pristine100nmParticles

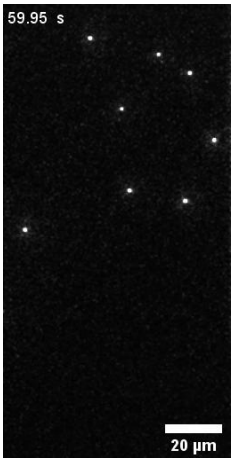

100 nm pristine particles added to lipid bilayers and imaged using total internal reflection microscopy. Bright spots indicate particles on/near the bilayer. Many particles can be seen adsorbing for long periods of time (50 ms frame rate). Snapshot depicted.

Supplementary video 2: SupplementaryVideo_S2_HardCorona100nmParticles

100 nm hard corona particles added to lipid bilayers and imaged using total internal reflection microscopy. Bright spots indicate particles on/near the bilayer. Some particles can be seen adsorbing for long periods of time whilst others desorb rapidly from the bilayer (50 ms frame rate). Snapshot depicted.

Supplementary video 3: SupplementaryVideo_S3_FullCorona100nmParticles

100 nm full corona particles added to lipid bilayers and imaged using total internal reflection microscopy. Bright spots indicate particles on/near the bilayer. Particles can be seen adsorbing and for very short periods of time before desorbing from the membrane (50 ms frame rate). Snapshot depicted.

References

1 N. G. van Kampen, in *Stochastic Processes in Physics and Chemistry (Third Edition)*, ed. N. G. Van kampen, Elsevier, Amsterdam, 2007, pp. 193–218.

2 N. Feliu, X. Sun, R. A. Alvarez Puebla and W. J. Parak, *Langmuir*, 2017, **33**, 6639–6646.

3 J.-Y. Tinevez, N. Perry, J. Schindelin, G. M. Hoopes, G. D. Reynolds, E. Laplantine, S. Y. Bednarek, S. L. Shorte and K. W. Eliceiri, *Methods*, 2017, **115**, 80–90.

4 C. A. Schneider, W. S. Rasband and K. W. Eliceiri, *Nature Methods*, 2012, **9**, 671–675.

5 J. Schindelin, I. Arganda-Carreras, E. Frise, V. Kaynig, M. Longair, T. Pietzsch, S. Preibisch, C. Rueden, S. Saalfeld, B. Schmid, J.-Y. Tinevez, D. J. White, V. Hartenstein, K. Eliceiri, P. Tomancak and A. Cardona, *Nature Methods*, 2012, **9**, 676–682.